

Dielectronic recombination of W^{20+} ($4d^{10}4f^8$): addressing the half-open f-shell

N. R. Badnell,¹ C. P. Ballance,² D. C. Griffin,³ and M. O'Mullane¹

¹*Department of Physics, University of Strathclyde, Glasgow G4 0NG, United Kingdom*

²*Department of Physics, Auburn University, Auburn, Alabama 36849*

³*Department of Physics, Rollins College, Winter Park, Florida 32789*

(Dated: April 11, 2012)

A recent measurement of the dielectronic recombination (DR) of W^{20+} [Schippers *et al* Phys. Rev. A **83**, 012711 (2011)] found an exceptionally large contribution from near threshold resonances ($\lesssim 1$ eV). This still affected the Maxwellian rate coefficient at much higher temperatures. The experimental result was found to be a factor 4 or more than that currently in use in the 100 – 300 eV range which is of relevance for modeling magnetic fusion plasmas. We have carried-out DR calculations with AUTOSTRUCTURE which include all significant single electron promotions. Our intermediate coupling results are more than a factor of 4 larger than our *LS*-coupling ones at 1 eV but still lie a factor 3 below experiment here. If we assume complete (chaotic) mixing of near-threshold autoionizing states then our results come into agreement (to within 20%) with experiment below $\lesssim 2$ eV. Our total IC Maxwellian rate coefficients are 50–30% smaller than those based-on experiment over 100–300 eV.

PACS numbers: 34.80.Lx, 34.80.Kw

I. INTRODUCTION

Tungsten will be a key element [1] in the ITER magnetic fusion device [2–4] currently under construction at Cadarache in France [5]. Its ability to withstand high power-loads means that it will be the primary facing material within the vacuum vessel. Its high nuclear charge means also that it is potentially a serious contaminant in the sense of its ability to quench the fusion reaction due to radiative power loss. Intensive studies are underway at all of the world's major magnetic fusion laboratories to understand, predict, and control its behavior. The recent ITER-like wall upgrade at JET [6] provides the closest reactor environment short of ITER itself. The 74 ionization stages of tungsten may seem daunting from the detailed theoretical perspective. Reality is somewhat different. Very few ionization stages are observed in practice. Near neutrals are seen as they sputter-off surfaces. Then many ionization stages burn through quite rapidly before ions of much higher charge-state are observed in particular localized environments. W^{20+} is a significant stage for spectral diagnostics and is seen at the null point of the separatrix at JET. W^{44+} performs a similar function at the core and is observed by the JET KX1 spectrometer. The ionization stages will change with the much larger and hotter ITER device but the principle remains the same: very few stages need to be modeled in detail. The great bulk of them can be modeled more 'coarsely' as superstages. Detailed studies are being made of these key stages. One of the most basic and important theoretical quantities is the tungsten ionization balance since it is the main determinant of the intensity of spectral line emission. Electron-collisional equilibrium is a balance between electron-impact ionization and dielectronic recombination. (All other recombination processes are negligible in the magnetic fusion domain.) A sufficiently accurate theoretical description of dielectronic recombination is key.

nation is key.

A recent experiment on W^{20+} ions by Schippers *et al* [7] at the TSR storage ring at Heidelberg measured an exceptionally large dielectronic recombination merged-beams 'rate coefficient' at a few eV. So-much-so that its contribution at the temperatures of significant fractional abundance for W^{20+} (100–300 eV) gave rise to a Maxwellian rate coefficient that is a factor 4 or more larger than that currently used by the main magnetic fusion modeling package — the Atomic Data and Analysis Structure (ADAS) [9]. We seek to resolve this discrepancy.

There is little previous detailed work on DR for f-shell ions. At one end ($4d^{10}4f$) there are calculations for Gd^{17+} by Dong *et al* [10] utilizing the Flexible Atomic Code (FAC) [11] which are relevant for modeling soft X-ray lithography. At the other end ($4d^{10}4f^{13+}$) there are calculations for Au^{20+} by Ballance *et al* [12] with AUTOSTRUCTURE [13]. The results of Ballance *et al* are in good agreement with the measurements of Schippers *et al* [8] from 2 meV up to 10 eV. Both of the above approaches are standard level-resolved calculations which allow for single electron promotions-plus-capture. They are largely restricted to at most doubly-excited configurations and interactions thereof.

Previous work on open f-shell ions is apparently limited to the configuration average approximation, the Burgess General Program (BBGP) [14, 15], and others of that ilk which are the mainstay of modeling codes. The calculations of Flambaum *et al* [16] for the DR of Au^{25+} (which is isoelectronic with W^{20+}) can be viewed as a form of partitioned configuration average. They utilize expressions for the radiative rate and autoionization rate which are similar to those of the configuration average. The near-threshold autoionization rates are partitioned over a Breit-Wigner distribution which is characterized by a single spreading width [17]. This compares with

our previous configuration average work [18] which partitions them over the non-metastable core levels according to their statistical weight. Such a partitioning maintains the allowed- vs forbidden-channel nature which is characteristic of DR in simple systems. The justification of the Breit-Wigner form and the spreading width follows from the complexity of the open f-shell ions in which configuration mixing tends to a chaotic limit which can be described by statistical theory [19]. This leads to a structureless continuum for the near-threshold merged-beams DR rate coefficient. The Au^{25+} results of Flambaum *et al* [16] were found to be in good agreement with the measurements of Hoffknecht *et al* [20] below 1 eV.

The approach to DR reported-on in this paper is a detailed (level-to-level) one with single electron promotions-plus-capture for all significant contributing configurations. The configuration mixing (and spin-orbit mixing) that we allow-for is the same as done in our previous work on the open Fe M-shell ($3p^q$) [21] and the open Sn N-shell ($4d^q$) [22] ions. This allows for the mixing of all autoionizing configurations within the $(N + 1)$ -electron complex when the promoted and captured electrons have the same principal quantum number. The inequivalent case restricts the mixing to configurations of the N -electron core i.e. with common Rydberg nl quantum numbers. This approach gives rise to a near-structureless continuum for the near-threshold merged-beams DR rate coefficient for these Fe and Sn cases. We seek to extend this work to the half-open f-shell and to compare the near-threshold merged-beams DR rate coefficient with the measurements of Schippers *et al* [7]. We seek also to determine the high energy Maxwellian DR rate coefficient applicable to the diagnostic modeling of W^{20+} in magnetic fusion plasmas.

We provide a description of our background theory in Sec. II. We describe its application to W^{20+} in Sec. III. We present our results and compare them with those of experiment in Sec. IV. We make some concluding remarks in Sec. V.

II. THEORY

We use the independent processes and isolated resonance approximations to describe dielectronic recombination [14]. The oft-repeated working equations may be found in [21] along with a more expansive discourse on the methodology we employ. We summarize some pertinent points.

A. Methodology

We use the computer code AUTOSTRUCTURE [13] to calculate all relevant atomic parameters: energy levels, radiative rates, and autoionization rates. A multi-configuration expansion is used in an LS -coupling or intermediate coupling (IC) representation. The configura-

tion average (CA) representation [23, 24] is a simpler approach which is very useful for complex heavy species since it provides a rapid overview of the problem.

All of our previous works with the CA approximation utilized the DRACULA code [24, 25]. One immediately sees the effect of level-resolution and fine-structure mixing when comparing LS -coupling with IC results obtained with AUTOSTRUCTURE. Comparison of LS -coupling with CA results has been clouded by the fact that DRACULA is based upon the Cowan structure code [26]. The Cowan code utilizes kappa-averaged Hartree-Fock radial orbitals [27]. The differences here with AUTOSTRUCTURE can be minimized by its use of kappa-averaged orbitals computed in self-consistent configuration average model potentials [26]. The Cowan code generally also scales various operator interactions¹. This facility is not readily or generally available in AUTOSTRUCTURE. We have implemented the CA angular momentum representation within AUTOSTRUCTURE. This eliminates any uncertainty in seeing the pure effect of moving to a configuration-mixed term-resolved representation. We have carried-out detailed CA comparisons between AUTOSTRUCTURE and DRACULA in the course of the present work so as to verify the integrity of the new development.

B. Computation

The (near-) half-open f-shell problem is a daunting one. If we view it simply in terms of binomial coefficients for the number of states present in a configuration then moving from the $4d^{10}4f^{13}$ ground configuration considered in [12] to $4d^{10}4f^8$ increases the number of states by a factor $(429/2)$. Memory requirements (CPU and disk) scale as $(429/2)^2$ and the time requirement as $(429/2)^3$. This is all relative. Absolute numbers are much larger once we start promoting electrons from the $4d$ - and $4f$ -subshells of the ground configuration. (The only bonus of the binomial effect is that $4f^7$ is only marginally worse than $4f^8$ since the number of states increases only by a factor $8/7$.)

The published AUTOSTRUCTURE code [13] was used for our recent work on the tin half-open d-shell [22] and $\text{Au}^{20+}4f^{13}$ [12]. It does not scale to the half-open f-shell. Substantial development has been necessary. A detailed exposition is more suited to a computer physics journal and so we give only a flavor here.

Most angular momentum packages used by atomic structure and collision codes are based upon Racah algebra. This is a hierarchical coupling scheme. A complication for the open f-shell is the need to introduce a new quantum number: seniority. AUTOSTRUCTURE employs the non-hierarchical Slater-state approach to angu-

¹ It does not do so under CA operation.

lar momentum coupling that was advocated by Condon and Shortley [28]. It has no concept of parentage². All interactions are expanded and determined initially in an uncoupled (Slater-state) representation. A transformation is then made to an LS and/or LSJ representation through the use of vector-coupling coefficients (VCCs). The half-open f-shell requires billions of coefficients and so tens of Gbytes of RAM per processor. They are not all required at the same time. It has been possible to implement an archival on disk in such a way that does not swamp the calculation with I/O.

Another issue concerns the large number of radiative and autoionization rates that arise in a level-resolved calculation. The approach to-date has been to archive them all to disk for subsequent processing in a variety of ways: to compare with experiment, to generate total rate coefficients for astrophysical modeling, or to process as final-state resolved data for collisional-radiative modeling for magnetic fusion. Such general flexibility comes at the cost of many Tbytes of disk space and corresponding I/O time. If we sacrifice some degree of generality then we can carry-out bundling over quantum numbers and summation of partial widths on-the-fly as the atomic data is generated. This reduces the data files to a manageable size. The user choice of bundling and/or summation should be guided by the exact same implementation made within the collisional-radiative modeling approach so as to render it tractable for heavy species. It is important to note that this introduces *no* additional approximation for our description of the experimental DR cross section nor the total Maxwellian rate coefficients presented later.

We do not dwell on various RAM and CPU time issues that arose as well on scaling from the open d- to f-shell. It is sufficient to note that the calculations reported-on below took about two weeks on a modest cluster (the problem does not engender large-scale parallelization) with 4Gb RAM and 250Gb of scratch disk per processor.

C. Mixing

We discuss the role of (configuration) mixing of autoionizing states on DR in complex heavy species. This is important since we include only a limited amount (see the next section). Consider a model problem in which we include only autoionizing configurations which result from single electron promotions-plus-capture from the the ground configuration. We assume that the autoionization rates (A_1) and radiative rates (R) satisfy $A_1 \gg R$. Then the DR cross section is basically proportional to R for a fixed symmetry. (We consider only autoionizations which are inverses of the dielectronic capture in this model i.e. near-threshold.) Now consider the

addition of autoionizing configurations which result from double electron promotions-plus-capture from the ground configuration. This set is only populated by mixing with the first via a unitary transformation. We denote the second set of autoionization rates by A_2 and assume similar radiative rates (R). We assume $A_2 \ll R$. If mixing between the two sets is strong enough and there are enough states then the autoionization rates for the first set (which we label now as A_{12}) are depleted to the extent that $A_{12} \ll R$. The DR cross section is now proportional to $A_{12} + A_2 = A_1$. The total is *enhanced* by a factor A_1/R . (Mixing only takes place between states of the same statistical weight and so the sum over autoionizing states is assumed to be implicit.) We consider the effect of further mixing. Now add configurations which result from triple electron promotions-plus-capture from the ground configuration. Denote the autoionization rates for the three sets as A_{123} , A_{23} , and A_3 . Assume all $A_i \ll R$ still. The total DR cross section is unchanged since it is proportional to $A_{123} + A_{23} + A_3 = A_1$ still. Such mixing is merely *redistributive* and so can be neglected with respect to total DR.

This is the nature of the near-threshold DR problem in complex ions described by Flambaum *et al* [16] (for Au^{25+}) following a preliminary earlier study [17]. The chaotic fully-mixed nature of Au^{24+} was verified by Gribov and Sahoo [29] who performed large-scale calculations of eigen-energies and eigen-vectors. Our detailed description of the autoionizing spectrum is necessarily incomplete. The above discussion is intended to shed light on how far we need to go. The model problem was merely illustrative in using configuration mixing via different sets of promotions. We are largely restricted to one electron promotions-plus-capture since we need to compute autoionization rates and radiative rates which are applicable over a much wider range of energies. But we do have differing representations: CA, LS -coupling and IC. The question then is one of the degree to which the IC representation is incomplete with regards to enhancement or whether it has moved to a redistributive regime so that our DR cross sections will have converged largely with respect to the total. The structured behavior of our low energy cross section, its comparison with experiment, and with statistical theory will enable us to judge the degree to which this is so. (It is straightforward to apply the statistical approach to our data — we simply partition our autoionization rates using the Breit-Wigner distribution — but note that this procedure is only valid near threshold.)

III. APPLICATION

The ground configuration of W^{20+} is $[\text{Kr}]4d^{10}4f^8$. The ground term is 7F . The ground level is $J = 6$. These denote the ground state of the CA, LS -coupling, and IC representations. We describe the DR reactions that we take account-of by their configuration representation.

² It is both possible and advantageous to introduce some parentage but it is not required.

This consists of N -electron configurations to which a continuum electron and a Rydberg electron are each coupled. This describes dielectronic capture and/or autoionization. The latter describes radiative transitions within the core also. Additional $(N + 1)$ -electron ‘correlation’ configurations are added to describe Rydberg electron radiation into the core. Rydberg–Rydberg radiation $n \rightarrow n' > 4$ is described hydrogenically. We breakdown the problem by target subshell promotion.

A. $\Delta n = 0$

We allow for $4d \rightarrow 4f$ and $4f \rightarrow 4f$ promotions in both LS -coupling and IC. The latter promotion does not contribute to CA DR since it corresponds to an elastic transition. The N -electron configurations are $4d^{10}4f^8$ and $4d^94f^9$. The $(N + 1)$ -electron configurations are $4d^{10}4f^9$ and $4d^94f^{10}$. We note that some terms/levels of $4d^{10}4f^75l$ lie below $4d^94f^9$. The former could provide an alternative autoionization channel for the latter. Such a transition is forbidden directly since it is described by a two-body operator. (A continuum electron is still to be coupled to the former and a Rydberg to the latter.) It could take place via mixing if we were to include additional configurations. We do not. We consider also the $4p \rightarrow 4f$ promotion in CA only. Its contribution is expected to be small. We normally use the CA calculation to determine the range of Rydberg- nl required to converge the total DR and then use these values subsequently for the more demanding LS -coupling and IC calculations. We find that the contribution to the Maxwellian rate coefficient from the $4d \rightarrow 4f$ promotion is converged to about 3% by $n = 100$ and $l = 7$ at all energies. It is not possible to do so for the $4f \rightarrow 4f$ promotion since the CA result is zero and so we utilize the LS -coupling calculation here to delimit the IC one. We find that the contribution from the $4f \rightarrow 4f$ promotion is converged to about 3% by $n = 100$ and $l = 6$ at all energies.

B. $\Delta n = 1$

We consider the $4d$ and $4f$ promotions separately.

1. $4f \rightarrow 5l$

The N -electron configurations are $4f^8$ and $4f^75l$ ($l = 0 - 4$). It is necessary to omit the $n = 5$ continuum so as to keep the problem tractable in the LS -coupling and IC calculations³. We carried-out CA calculations both with

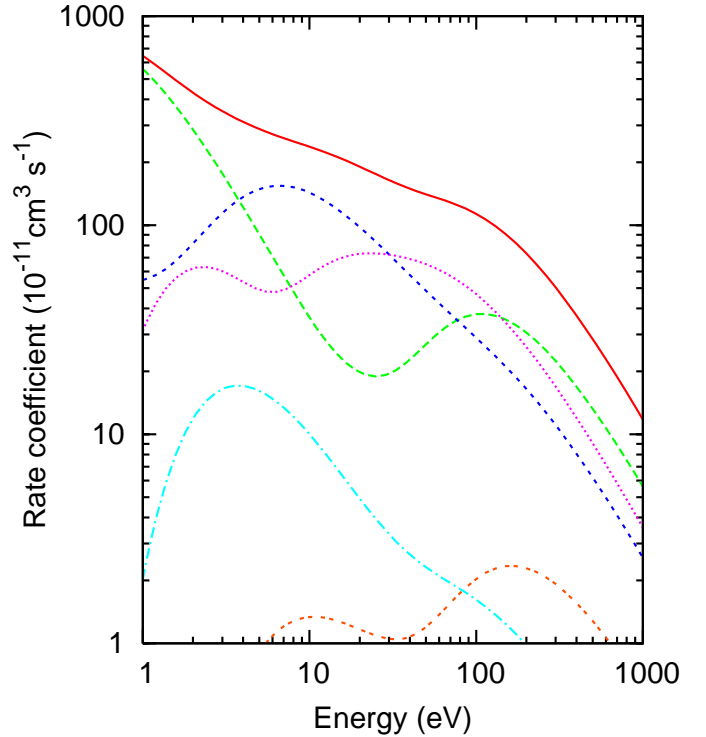


FIG. 1: (Color online) W^{20+} CA Maxwellian DR rate coefficient contributions for various promotions: total (solid red curve), $4d \rightarrow 4f$ (long-dashed green curve), $4f \rightarrow 5l$ (short-dashed blue curve), $4d \rightarrow 5l$ (dotted magenta curve), $4p \rightarrow 4f$ (dot-dashed cyan curve), and $4d + 4f \rightarrow 6l$ (double-dashed orange curve).

and without the $n = 5$ continuum to aid our analysis of the uncertainty (overestimate) in our LS -coupling and IC results. There is none at all below ~ 20 eV since they are all energetically closed.

The $(N + 1)$ -electron configurations are $4f^85l$ ($l = 0 - 4$). Some of the $4f^75l5l'$ configurations are (partially) bound. We treat such $n \rightarrow n' = 5$ radiation hydrogenically (approximately) in the LS -coupling and IC calculations. They are either strictly bound or autoionizing in the CA approximation. Their contribution is small.

The CA results for this promotion are converged to about 5% at 200eV and 10% at 1000 eV on summing to $l = 5$. The sum over n is converged to better than 2% by $n = 100$. We add this small ‘top-up’ in l (and n since we are doing so) from our CA results to the LS -coupling and IC ones.

³ The number of VCCs that need to be internally buffered becomes too large. A smaller buffer could be implemented but this would

likely increase I/O time substantially. The absolute number of VCCs required in LS -coupling is only typically a factor of 2 smaller than for IC. The demands of the IC calculation arise from the fact that far more of the states that they represent interact.

2. $4d \rightarrow 5l$

The N -electron configurations are $4d^{10}4f^8$, $4d^94f^9$, $4d^94f^85l$ ($l = 0 - 4$) and $4d^{10}4f^75l$ ($l = 0 - 4$). We omit the $n = 5$ continuum again. The $4d^94f^8$ is rather demanding when coupled to $5lnl'$ for $l + l' > 5$. It has a factor $70/8$ more states than the corresponding $4d^{10}4f^7$. We need to consider it further. We write the dielectronic capture reaction in a somewhat unusual form:

$$4f^8(^7F)4d^{10} + e^- \rightarrow 4f^8(^7F)4d^95lnl'.$$

This illustrates the role of the $4f^8(^7F)$ ground term as a spectator. It cannot change simultaneously with the two-body dielectronic capture. It can change (shake-up) via mixing in the autoionizing states. We omit such mixing. We do the same for the reverse radiative stabilization to $4f^8(^7F)4d^{10}nl$. This renders a tractable but reasonable description of the $4d \rightarrow 5l$ promotions. We recall that there is no configuration mixing whatsoever present in the CA approximation. We recall also the lack of sensitivity to configuration mixing that we found for total DR in the tin $4p - 4d$ transition array despite the demonstrable extensive configuration mixing [22]. Such an argument may not be valid near threshold — see the discussion in Sec. II C. We emphasize that we place no such restrictions (on mixing) when the $4f$ is active such as for the $4d^94f^9$ configuration. We have implemented the general user specification of term restrictions for spectator subshells within AUTOSTRUCTURE. These are common to all configurations which contain the specified subshell(s).

The $(N + 1)$ -electron configurations are $4d^{10}4f^85l$ ($l = 0 - 4$) and $4d^94f^95l$ ($l = 0 - 4$). A few of the $4d^94f^85l5l'$ configurations are (partially) bound and we treat them as for $4f \rightarrow 5l$.

The CA results for this promotion are converged to 1% at 1000 eV on summing to $l = 4$. The sum over n is converged to much better than 1% by $n = 100$.

C. $\Delta n = 2$

We consider $4d + 4f \rightarrow 6l$ promotions within the CA approximation only. The contribution is expected to be small.

IV. RESULTS

We show an overview of the different CA contributions to the total DR Maxwellian rate coefficient in Fig. 1. The energy range of interest for an electron collisional plasma is 100–300 eV. This is where W^{20+} has its maximal fractional abundance (> 0.01) in a magnetic fusion plasma.

We remark that the contribution from $4d \rightarrow 4f$ promotions is comparable with the $\Delta n = 1$ above ~ 100 eV. This is in contrast to case of the almost full $4f$ -subshell case of Au^{20+} [12]. It also dominates at a few eV but this behavior can be expected to be more ion-dependent.

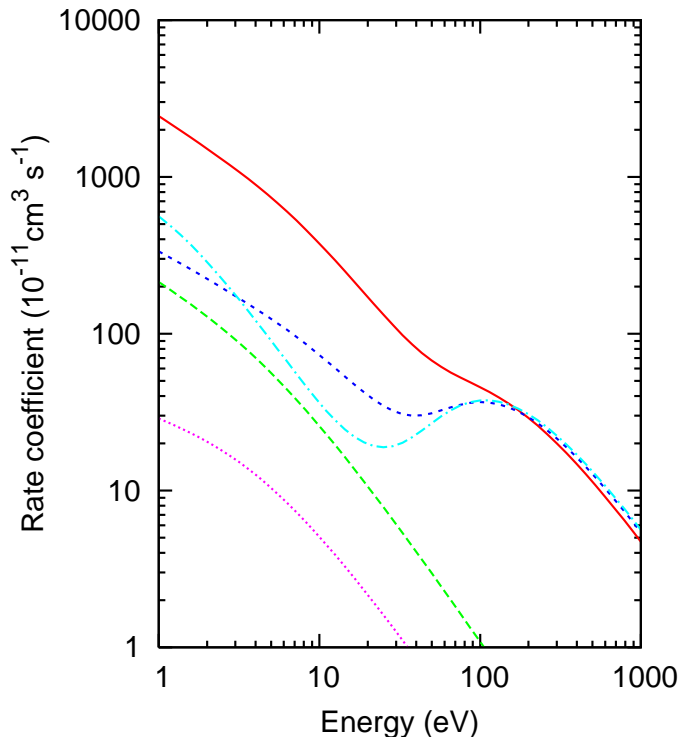


FIG. 2: (Color online) W^{20+} Maxwellian DR rate coefficient contributions for $\Delta n = 0$ promotions: IC $4d \rightarrow 4f$ (solid red curve), IC $4f \rightarrow 4f$ (long-dashed green curve), LS $4d \rightarrow 4f$ (short-dashed blue curve), LS $4f \rightarrow 4f$ (dotted magenta curve), and CA $4d \rightarrow 4f$ (dot-dashed cyan curve).

We see that we do not need to consider $4p \rightarrow 4f$ and $\Delta n = 2$ promotions any further.

A. $\Delta n = 0$

We present and compare our LS -coupling and IC results for the $4f \rightarrow 4f$ and $4d \rightarrow 4f$ promotions in Fig. 2. We note the close agreement between them and the CA results for the $4d \rightarrow 4f$ promotion above ~ 100 eV. There is about a factor 7 difference between the LS -coupling and IC results down at 1 eV. The contribution from the $4f \rightarrow 4f$ is no more than about 10% of the $4d \rightarrow 4f$ above 1 eV.

B. $\Delta n = 1$

1. $4f \rightarrow 5l$

We present and compare our LS -coupling and IC results for the $4f \rightarrow 5l$ promotions in Fig. 3. We separate-out the contributions from capture to $n = 5$ and $n > 5$. The sum of the two in LS -coupling and IC agree to within 10% by 100 eV. We show CA results both with and without autoionization to the $n = 5$ continuum. The rather

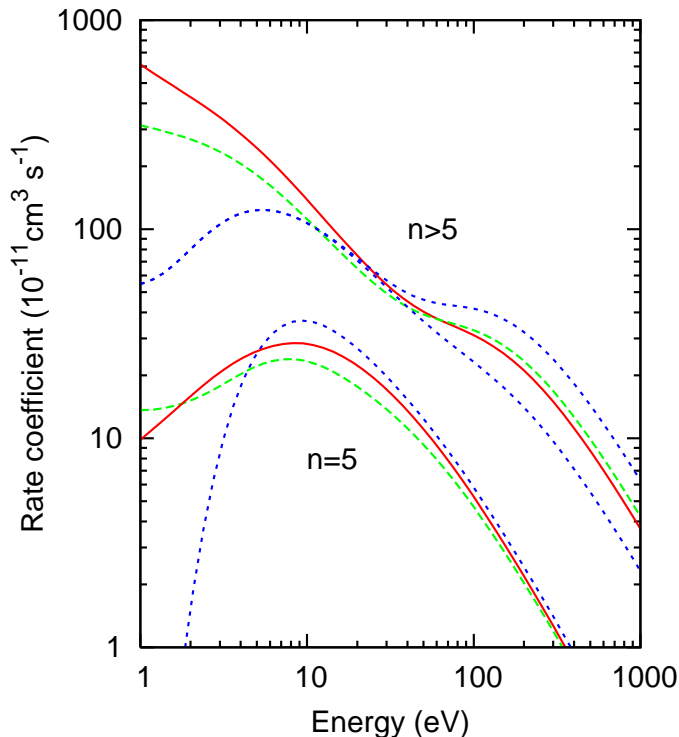


FIG. 3: (Color online) W^{20+} Maxwellian DR rate coefficient contributions for $4f \rightarrow 5l$ ($l = 0 - 4$) promotions (capture to $n = 5$ and $n > 5$ are shown separately): IC (solid red curves), LS (long-dashed green curves), and CA, $n > 5$ both with and without the $n = 5$ continuum (short-dashed blue curves).

pronounced high energy peak is reduced by a factor of 2 at 160 eV. These are the first autoionizations into excited states pathways in the CA coupling scheme. The LS -coupling and IC are already suppressed by autoionization into (the continuum of) a multitude of excited states within the ground configuration. This is reflected in their less pronounced high energy peaks. We would not expect the ($n > 5$) LS -coupling and IC results to be suppressed further by more than $\sim 20\%$ below 300 eV.

2. $4d \rightarrow 5l$

We present and compare our LS -coupling and IC results for the $4d \rightarrow 5l$ promotions in Fig. 4. We see that the relative contributions from capture to $n = 5$ and $n > 5$ are reversed compared to the $4f \rightarrow 5l$ promotions. The $n > 5$ contribution does not exceed that of the $n = 5$ until high energy. This is due to autoionization suppression via the $4f \rightarrow 4d$ inner-shell transition. The CA results for $n > 5$ are suppressed by a factor of two at 160 eV but the sum including $n = 5$ by about one third. The ($n > 5$) LS -coupling and IC results are likely to be suppressed by a larger relative factor than for the case of $4f \rightarrow 5l$ promotions but the overall sum including $n = 5$ dilutes the factor and $\sim 20\%$ appears to be a reasonable

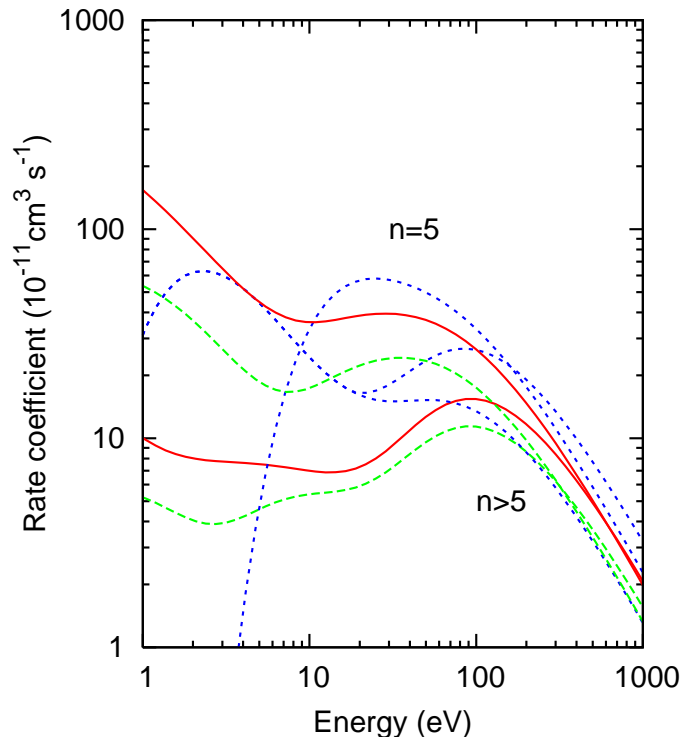


FIG. 4: (Color online) W^{20+} Maxwellian DR rate coefficient contributions for $4d \rightarrow 5l$ ($l = 0 - 4$) promotions (capture to $n = 5$ and $n > 5$ are shown separately): IC (solid red curves), LS (long-dashed green curves), and CA, $n > 5$ both with and without the $n = 5$ continuum (short-dashed blue curves).

estimate here.

C. Totals (Merged-beams)

We convoluted our DR cross sections with the electron velocity distribution applicable for the merged electron beams in the TSR cooler [7]. We compare our resultant total DR rate coefficients with those measured on the TSR storage ring [7]. We focus first on the near threshold region [0–10] eV for which Schippers *et al* reported the largest measured DR rate coefficient to-date. We see in Fig. 5 that our IC results are a factor 2–5 larger than our LS -coupling ones but they are still typically a factor of 3 smaller than experiment. Our IC results are dominated by the $4d \rightarrow 4f$ promotion (80%). The density of resonances is such that there is little resultant structure in the total. We have a near quasi-continuum of resonances. It does not matter then just where the ionization limit lies.

The remaining factor of ~ 3 is likely due to the incomplete mixing within our IC configuration expansion. We show results (Fig. 5) where we have partitioned our autoionization rates using the Breit-Wigner distribution with a spreading width of 10 eV [17]. The results are not particularly sensitive to this width. Our CA, LS -coupling

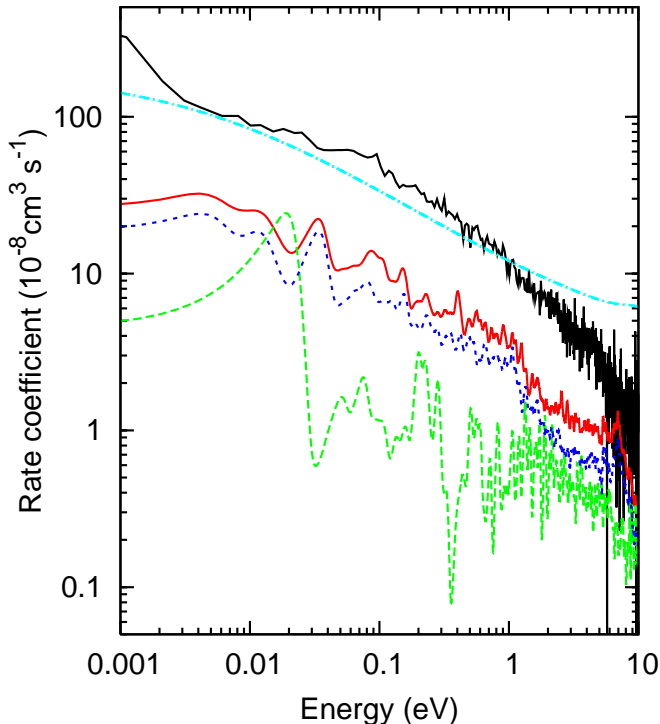


FIG. 5: (Color online) W^{20+} merged-beams DR rate coefficients: experiment [7] (solid black curve), partitioned total (dot-dashed cyan curve), IC total (solid red curve), LS total (long-dashed green curve), and IC $4d \rightarrow 4f$ only (short-dashed blue curve).

and IC results are barely distinguishable on this scale and so we show a single curve. We obtain agreement with experiment to within 20% over 0.003 – 2 eV. Similar findings were obtained by Flambaum *et al* [16] for Au^{25+} . (The measured cross section increases at energies below 0.003 eV due to an artifact of the merged-beams technique [30].)

The first excited level of the ground term opens-up just below 2 eV. The experimental cross section falls away progressively thereafter — see Fig. 6. This fall-off coincides with an increasing number of alternative autoionization channels opening-up. If autoionization into excited levels is fully redistributed as per the ground then the total width is unaffected. The partitioned autoionization widths to the ground level are orders of magnitude smaller than the radiative widths. This is why the partitioned results are largely unchanged — even when summing over autoionization to hundreds of excited levels. In nature it would appear that typical autoionizing widths to the ground level are no more than a factor ~ 10 smaller than the radiative widths. Summing over a relatively small number of excited continua then produces a total autoionization width comparable with and then exceeding the radiative width. We note that our level-resolved autoionization widths are only typically at most a factor 5–10 larger than the radiative widths. Ex-

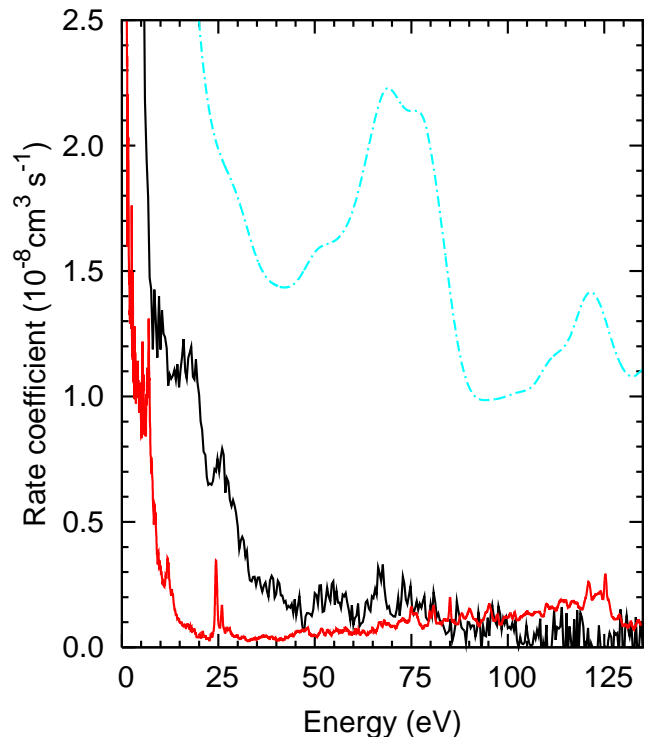


FIG. 6: (Color online) W^{20+} merged-beams DR rate coefficients: experiment [7] (solid black curve), partitioned total (dot-dashed cyan curve), IC total (solid red curve).

periment falls between the two theoretical ‘limits’. The partitioned results are clearly inapplicable here.

All of our results are an upper limit because we assume 100% of the W^{20+} initial ion population to be residing in the ground state. Schippers *et al* [7] identify several possible metastable levels that could remain populated during the lifetime of the measurement but have no estimate of their population. Any combination of metastables that we take reduces the total. This is because DR from excited states is suppressed by autoionization into the continuum attached to lower levels. Only the ground level is immune from such. The agreement between our Breit-Wigner partitioned results and experiment below 10 eV would indicate that the metastable presence is not significant.

D. Totals (Maxwellian)

We turn now to the corresponding total Maxwellian DR rate coefficients. We compare results in Figs. 7 and 8. The two CA results (Fig. 7) illustrate the effect of omission of $n = 5$ continuum suppression on the total. It is 25% at 160 eV. The lower CA, *LS*-coupling, and IC results are all in close agreement above ~ 100 eV. The *LS*-coupling and IC results are an upper limit not just because of the omission of the $n = 5$ continuum but also because they assume 100% of the W^{20+} initial ion popu-

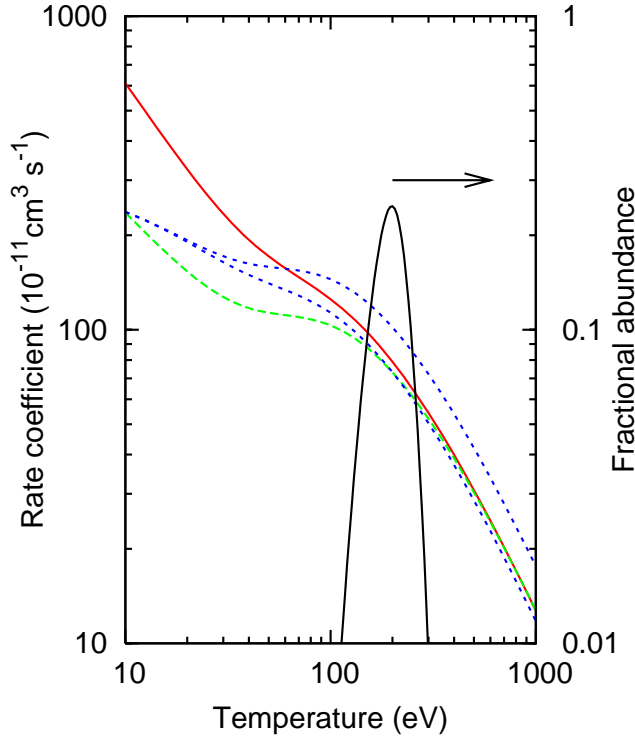


FIG. 7: (Color online) W^{20+} total Maxwellian DR rate coefficients: IC (solid red curve), LS (long-dashed green curve), and CA with-and-without $n = 5$ continuum (short-dashed blue curves). The fractional abundance of W^{20+} in a magnetic fusion plasma is shown also (solid black curve).

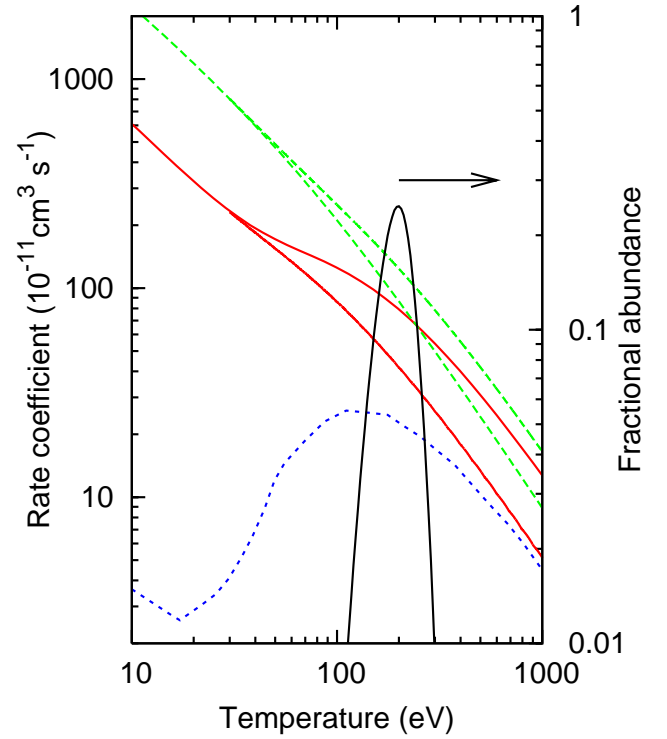


FIG. 8: (Color online) W^{20+} total Maxwellian DR rate coefficients: IC all resonances and to 140 eV only (solid red curves), experiment [7] to 140 eV and with theory top-up for resonances above 140 eV (long-dashed green curves), and ADAS [31] (short-dashed blue curve). The fractional abundance of W^{20+} in a magnetic fusion plasma is shown also (solid black curve).

lation to be residing in the ground state.

The experiment by Schippers *et al* [7] only detects resonances which occur below 140 eV. We show a second IC result (Fig. 8) which imposes such a cut-off. This cut-off result lies just over 50% below experiment at 160 eV. If we add a theoretical top-up (for the resonances above 140 eV) to the experimental result then this difference is reduced to about 40% (at 160 eV) and is 50–30% over 100–300 eV. The top-up is between 20–60% of the experimental result alone over 100–300 eV. The topped-up experimental result is the total (zero-density) DR rate coefficient that we recommend for use in modeling because of the remaining difference between theory and experiment. This difference is attributable to the difference in the contribution from low energy resonances. The $\Delta n = 0$ resonances as a whole contribute about one third of the IC total at 160 eV. The factor 3 larger experimental contribution from such resonances at low energies means that they contribute significantly more here.

The final results we show in Fig. 8 are those from ADAS [31]. These were determined using the Burgess General Formula (GF) [32] — this is ADAS Case A [9] which extends the GF validity to finite density by the use of a global suppression factor [33]. Those shown here were determined at close to zero electron density (10^8 cm^{-3}).

We see that the ADAS [31] results lie between a factor 10 and 4.5 below our recommended ones over 100–300 eV. The ADAS results are for dielectronic plus radiative recombination. The radiative contribution dominates in these results below 20 eV because the Case A Burgess GF cannot describe the effect of low-lying resonances. Such low-lying resonances can be described by the the BBGP approach [14, 15] — this is ADAS Case B which resolves the final recombined state and so is amenable to the collisional-radiative modeling of density effects [34].

The fractional abundance curve we show has been determined using the ADAS Case A data at an electron density of 10^{13} cm^{-3} which is typical of that relevant to magnetic fusion edge plasmas [1]. It differs slightly from the one shown by Schippers *et al* [7] which is due to Pütterich [35] and at 10^{14} cm^{-3} . It is appropriate to use a finite-density abundance to indicate the plasma relevant temperatures on which to focus our comparisons of zero-density rate coefficients because the temperature of peak abundance is density sensitive. Use of rate coefficients which are up to a factor 10 larger though is likely to move the peak abundance to higher temperature. (Similar increases in the DR rates to used can be expected for adjacent ionization stages.)

TABLE I: Recommended total (zero-density) dielectronic recombination rate coefficient fitting coefficients c_i ($\text{cm}^3\text{s}^{-1}[\text{eV}]^{3/2}$) and E_i (eV) for the initial ground level of W^{20+} .

i	c_i	E_i
1	$4.025(-7)^a$	$1.093(+0)$
2	$7.697(-7)$	$9.153(+0)$
3	$1.065(-6)$	$3.425(+1)$
4	$1.487(-6)$	$1.205(+2)$
5	$2.177(-6)$	$2.384(+2)$

^a(m) denotes $\times 10^m$.

1. Density effects

A rigorous treatment of density effects on dielectronic recombination rate coefficients and their consequential effect on the ionization balance of W^{20+} and adjacent ionization stages is beyond the scope of the present work. We can make some observations though. The ADAS rate coefficient is reduced by a factor of 2 at an electron density of 10^{13} cm^{-3} (not shown) compared to zero-density. This is due to the stepwise ionization of high- n ($\gtrsim 10$) Rydberg states following recombination. The new recommended total DR rate coefficients contain a large contribution from low-energy resonances of low- n ($\lesssim 10$). If we assume that the high- n contributions to both are broadly similar then we can expect maybe a 10–20% reduction in the new recommended values over 100–300 eV. Similar (reduced) effects can be expected for adjacent ionization stages. This means that the corresponding fractional abundances are likewise less sensitive to the electron density than indicated by the current ADAS data. A revision of the density dependent ionization balance of f-shell tungsten ions is clearly needed.

2. Fitting coefficients

It is convenient often for simple modeling purposes to fit the total Maxwellian dielectronic recombination rate coefficient (α) to the following functional form:

$$\alpha(T) = T^{-3/2} \sum_i c_i \exp\left(\frac{-E_i}{T}\right)$$

where the E_i are in the units of temperature T (e.g. eV) and the units of c_i are then $\text{cm}^3\text{s}^{-1}[\text{eV}]^{3/2}$.

In Table I we present such fitting coefficients for the recommended (experiment topped-up by theory) total zero-density dielectronic recombination rate coefficient for the initial ground level of W^{20+} . The fit is accurate to better (often much better) than 1% over 1–1000 eV.

The total dielectronic recombination rate coefficient can be taken to be the total recombination rate coefficient. The contribution from radiative recombination is negligible over the given temperature range as is that from three-body recombination at the densities of interest to magnetic fusion plasmas.

V. CONCLUSION

We have calculated IC DR rate coefficients for W^{20+} which include all significant one-electron promotions-plus-capture. A factor 3 difference with experiment remains at low energies. We have demonstrated that this can be removed if we assume complete chaotic mixing of multiply-excited near-threshold configurations. A similar finding was obtained by Flambaum *et al* [16] for Au^{25+} . The difference between theory and (topped-up) experiment at energies relevant to magnetic fusion modeling for ITER is somewhat less viz. between a factor two and 1.5 over 100–300 eV. The DR data used by ADAS for such modeling needs to be updated since the current Burgess GF Case A results lie between a factor 10 and 4.5 below our new recommended values over 100–300 eV. Our CA, *LS*-coupling and IC results are all in close accord (20%) above 100eV which suggests that DR rate coefficients for complex W ions can be determined readily to within a factor of two for modeling purposes. Similar behavior can be expected for related complex ions of other heavy elements. Determination of such DR rate coefficients which are accurate to the $\sim 20\%$ level remains problematic though.

ACKNOWLEDGMENTS

We would like to thank Stefan Schippers for providing the experimental data in numerical form. One of us (NRB) would like to thank Gleb Gribakin for clarifying the methodology used in [16]. This work was supported in part by a Euratom Framework 7 Support Action Agreement with the University of Strathclyde and US DoE grants to Auburn University.

-
- [1] T. Pütterich, R. Neu, R. Dux, A. D. Whiteford, M. G. O'Mullane, and the ASDEX Upgrade Team, Plasma Phys. Control. Fusion **50** 085016(27) (2008).
 - [2] <http://www.iter.org>
 - [3] ITER Physics Basis *Nucl. Fusion* **39** 2137–74 (1999).
 - [4] R. Aymar, P. Barabaschi and Y. Shimomura (for the

ITER Team), Plasma Phys. Control. Fusion **44** 519–65 (2002).

- [5] <http://en.wikipedia.org/wiki/Cadarache>
- [6] <http://www.efda.org/jet/>
- [7] S. Schippers, D. Bernhardt, A. Müller, C. Krantz, M. Grieser, R. Repnow, A. Wolf, M. Lestinsky, M. Hahn, O.

- Novotný, and D. W. Savin, Phys. Rev. A **83**, 012711(6) (2011).
- [8] S. Schippers, D. Bernhardt, M. Grieser, M. Hahn, C. Krantz, M. Lestinsky, O. Novotný, R. Repnow, D. W. Savin, A. Wolf, and A. Müller, Phys. Scr. **T144**, 014039(3) (2011).
- [9] H. P. Summers, *The ADAS User Manual v2.6* (2004); <http://www.adas.ac.uk>
- [10] C. Z. Dong, Private Communication (2011).
- [11] M. F. Gu, Can. J. Phys. **86**, 675–89 (2008).
- [12] C. P. Ballance, D. C. Griffin, S. D. Loch, and N. R. Badnell, J. Phys. B At Press (2012).
- [13] N. R. Badnell, Comp. Phys. Commun. **182**, 1528–35 (2011).
- [14] A. Burgess, Astrophys. J. **139**, 776–80 (1964).
- [15] N. R. Badnell, M. O’Mullane, H. P. Summers, Z. Altun, M. A. Bautista, J. Colgan, T. W. Gorczyca, D. M. Mitnik, M. S. Pindzola, and O. Zatsarinny, Astron. Astrophys. **406**, 1151–65 (2003).
- [16] V. V. Flambaum, A. A. Gribakina, G. F. Gribakin, and C. Harabati, Phys. Rev. A **66**, 012713(7) (2002).
- [17] G. F. Gribakin, A. A. Gribakina, and V. V. Flambaum, Aust. J. Phys. **52**, 443–57 (1999).
- [18] N. R. Badnell and M. S. Pindzola, Phys. Rev. A **39**, 1685–9 (1989).
- [19] V. V. Flambaum, A. A. Gribakina, G. F. Gribakin, and M. G. Kozlov, Phys. Rev. A **50**, 267–96 (1994).
- [20] A. Hoffknecht, O. Uwira, S. Schennach, A. Frank, J. Haselbauer, W. Spies, N. Angert, P. H. Mokler, R. Becker, M. Kleinod, S. Schippers, and A. Müller, J. Phys. B **31** 2415–28 (1998).
- [21] N. R. Badnell, J. Phys. B **39**, 4825–52 (2006).
- [22] N. R. Badnell, A. Foster, D. C. Griffin, D. Kilbane, M. O’Mullane, and H. P. Summers, J. Phys. B **44**, 135201(12) (2011).
- [23] M. S. Pindzola, D. C. Griffin, and C. Bottcher, *Atomic Processes in Electron–Ion and Ion–Ion Collisions NATO ASI B145*, 75–91 (1986).
- [24] D. C. Griffin, M. S. Pindzola, and C. Bottcher, Phys. Rev. A **31** 568–75, (1985).
- [25] C. P. Ballance, S. D. Loch, M. S. Pindzola, and D. C. Griffin, J. Phys. B **43**, 205201(9) (2010).
- [26] R. D. Cowan *The Theory of Atomic Structure and Spectra* (Berkeley, CA: University of California Press, 1981).
- [27] R. D. Cowan and D. C. Griffin, J. Opt. Soc. Am. **66**, 1010–4 (1975).
- [28] E. U. Condon and G. H. Shortley *The Theory of Atomic Spectra* (CUP, 1935).
- [29] G. F. Gribakin and S. Sahoo, J. Phys. B **36**, 3349–70 (2003).
- [30] G. Gwinner, A. Hoffknecht, T. Bartsch, M. Beutelspacher, N. Eklöw, P. Glans, M. Grieser, S. Kröhn, E. Lindroth, A. Müller, A. A. Saghir, S. Schippers, U. Schwamm, D. Schwalm, M. Tokman, G. Wissler, and A. Wolf, Phys. Rev. Lett. **84**, 4822–5 (2000).
- [31] A. Foster, *On the Behaviour and Radiating Properties of Heavy Elements in Fusion Plasmas*, Ph. D. thesis, University of Strathclyde, Glasgow, UK (2008).
- [32] A. Burgess, Astrophys. J. **141** 1588–90 (1965); A. Burgess and A. S. Tworkowski, Astrophys. J. **205** L105–7 (1976); A. L. Merts, R. D. Cowan, and N. H. Magee Jr, Los Alamos Scientific Laboratory Report LA-6220-MS (1976).
- [33] A. Burgess, Smithsonian Ap. Obs. Rept. **174**, 47–59 (1965) and (unpublished); B. W. Shore, Lawrence Livermore Laboratory Report UCIR-854 (1975).
- [34] A. Burgess and H. P. Summers, Astrophys. J. **157**, 1007–1021 (1969).
- [35] T. Pütterich, *Investigations on Spectroscopic Diagnostic of High-Z Elements in Fusion Plasma*. Ph. D. thesis, University of Augsburg, Germany (2005).